Available online at www.sciencedirect.com
ScienceDirect
International Journal of Multiphase Flow 33 (2007) 1222–1236
International Journal of Multiphase Flow
www.elsevier.com/locate/ijmulflow

Experimental study on a two-phase critical flow with a non-condensable gas at high pressure conditions

Hyun-Sik Park *, Nam-Hyun Choi, Seok-Kyu Chang, Chang-Hwan Chung, Sung-Jae Yi, Choon-Kyung Park, Moon-Ki Chung

Thermal Hydraulics Safety Research Center, Korea Atomic Energy Research Institute, 1045 Daedeokdaero, Yuseong, Daejeon, 305-600, Republic of Korea

Received 2 July 2006; received in revised form 7 May 2007

Abstract

An experimental study was performed on a two-phase critical flow with a non-condensable gas at high pressure conditions. Experimental data for the critical flow rates were generated by using sharp-edged stainless steel pipes with an inner diameter of 10.9 mm, a thickness of 3.2 mm, and a length of 1000 mm. The test conditions were varied by using the stagnation pressures of 4.0, 7.0, and 10.0 MPa, water subcoolings of 0.0, 20.0, and 50.0 °C, and nitrogen gas flow rates of 0.0–0.22 kg/s. The experimental results show that the critical mass flux decreases rapidly with an increase of the volumetric non-condensable gas fraction. Also the critical mass flux increases with an increase of the stagnation pressure and a decrease of the stagnation temperature. An empirical correlation of the non-dimensional critical mass flux, which is expressed as an exponential function of the non-condensable gas fraction of the volumetric flow, is obtained from the experimental data.

Keywords: Two-phase flow; Critical flow; Non-condensable gas; High pressure

1. Introduction

The discharge of a high-pressure and temperature fluid from a reactor coolant system is frequently encountered during the safety analysis of pressurized water reactors. SMART is an advanced integral type pressurized water reactor whose major components of the reactor coolant system are contained in a reactor vessel (Chang et al., 2002a,b) and whose thermal–hydraulic characteristics have been experimentally investigated (Choi et al., 2006). Recently one of the problems associated with the overall safety analysis of the SMART design has been an accurate prediction of the coolant discharge rate following a rupture of a connecting pipe. The SMART is equipped with a self-pressurizing pressurizer which uses nitrogen gas. During its operation the

* Corresponding author. Tel.: +82 42 868 8615; fax: +82 42 861 6438.
E-mail address: hspark@kaeri.re.kr (H.-S. Park).

0301-9322/$ - see front matter © 2007 Elsevier Ltd. All rights reserved.
doi:10.1016/j.ijmultiphaseflow.2007.05.008

pressurizer is filled with nitrogen gas, steam and water and it is connected to three gas cylinders via three penetrating pipes. If one of the connecting pipes is broken, a mixture of nitrogen gas, steam and water is discharged through that broken pipe. So it is very important to predict the critical flow rate of the discharged water with the non-condensable gas present.

Extensive experimental and theoretical researches have been carried out to clarify the two-phase critical flow phenomenon which occurs through a broken pipe following a loss of coolant accidents (LOCA) in pressurized water reactors by several researchers such as Moody (1965), Henry (1970), Wallis (1980), Trap and Ransom (1982), and Elias and Lellouche (1994). Especially Elias and Lellouche (1994) provided a general review of a two-phase critical flow from the viewpoint of the needs of these thermal–hydraulic systems codes and they conducted a systematic evaluation of the existing data and theoretical models in order to quantify the validity of the ten most widely used critical flow models against an extensive set of data from critical flow experiments. Some practical correlations for a two-phase critical flow were also provided. Fauske (1985) provided practical guidelines for estimating flashing flows and Park (1997) investigated the critical two-phase flow rates of a subcooled water through short pipes with small diameters for wide ranges of a subcooling and pressure and he developed empirical correlations for calculating the critical flow rate of a subcooled water. Recently Pinhasi et al. (2005) reviewed the flashing phenomena in a two-phase flow system of a single pure substance by focusing on the work done on predicting the release rates of hazardous materials from ruptured vessels containing such materials in the form of compressed liquids.

However, the influence of a non-condensable gas on a critical two-phase flow is not really understood and its experimental and theoretical investigations are rare. Celata et al. (1988) performed experiments at stagnation pressures of 0.5, 1.0, 1.5 MPa and inlet subcoolings of 0, 20, 40, 60 °C to study the influence of a non-condensable gas on a steam-water two-phase critical flow and they reported on an analysis of the effects of a non-condensable gas under different stagnation conditions. Air was used as the non-condensable gas and the test section was a round-edged pipe which had an inner diameter of 4.6 mm and a length of 1500 mm. Chang et al. (2002a,b) also performed a series of two-phase critical flow tests with a non-condensable gas at KAERI (Korea Atomic Energy Research Institute) by using a test section with an inner diameter of 20.0 mm and a length of 300 mm, to ascertain the effects of a non-condensable gas such as nitrogen gas on a critical flow at high pressure conditions. The critical flow data were produced to simulate a discharge of coolant with a non-condensable gas through a broken pipe during a small break loss of coolant accident in SMART (Chang et al., 2002a,b). The obtained experimental data were used to validate the existing two-phase critical flow model with a non-condensable gas and to develop a new model (Kim et al., 2002).

In this paper some of the experimental data for the two-phase critical flow rates for both with and without a non-condensable gas are presented. The empirical correlations for two-phase critical flow rates with a non-condensable gas are developed based on the acquired experimental data.

2. Description of the critical flow test facility

2.1. Configuration of the test facility

A non-condensable gas two-phase critical flow test facility was designed and constructed at KAERI to simulate a pipe break accident of an advanced integral reactor, SMART (Chang et al., 2002a,b). The non-condensable gas two-phase critical flow test facility is composed of a main circulation system, a coolant discharge system, a nitrogen gas supply system, and a nitrogen gas charging system. Fig. 1 shows a schematic diagram of the KAERI critical flow test facility.

The major components of the non-condensable gas two-phase critical flow test facility are a pressure vessel, a test section, a suppression tank, and a nitrogen gas supply system. The main circulation system has the functions of setting and maintaining the stagnation temperature and pressure at the required experimental conditions. This is possible by heating and pressurizing the coolant inside the pressure vessel, which is circulated in a circulation loop installed with a pump, an electrical heater, and a heat exchanger. The coolant discharge system has the function of producing the experimental data by discharging the coolant through the test section into the suppression tank. The nitrogen gas supply system has the function of pressurizing the pressure vessel to the pre-determined pressure and injecting the nitrogen gas into the upstream of the test section in the case

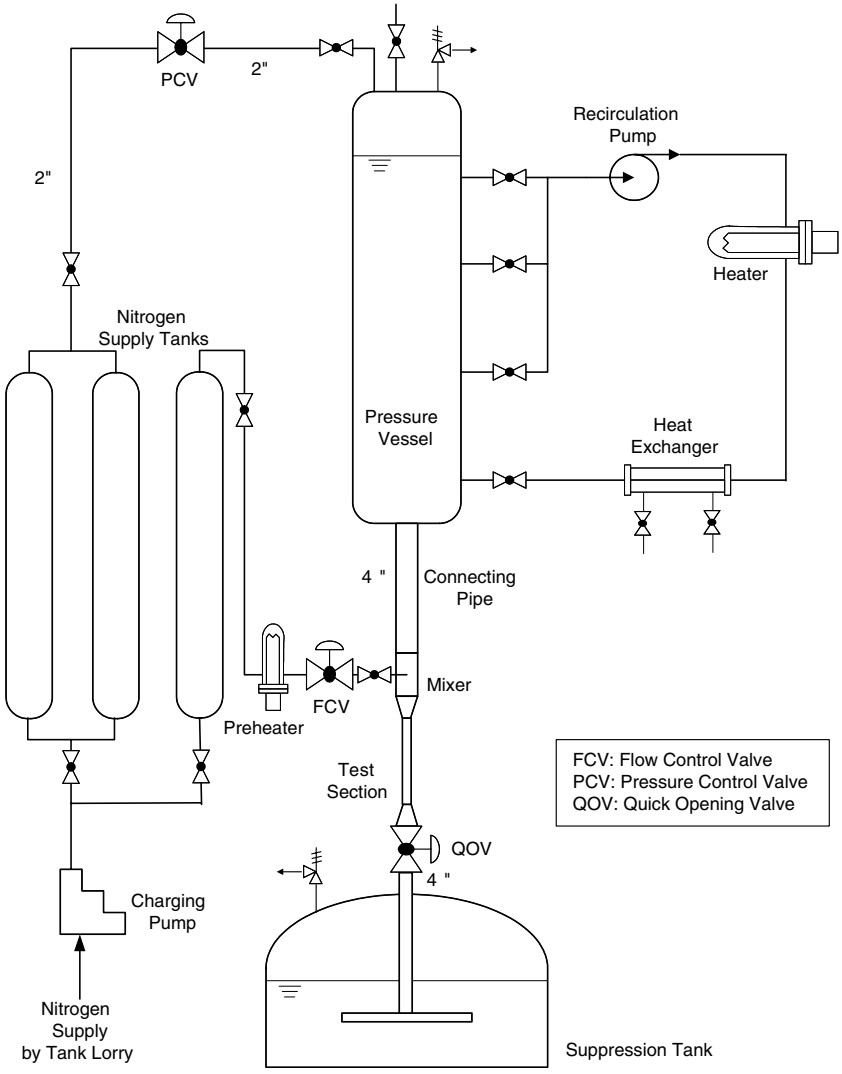

Fig. 1. Schematic of the KAERI Non-condensable gas two-phase critical flow test facility.

when a non-condensable gas is used. The nitrogen gas charging system has the function of charging the gas into the nitrogen gas supply tank by using a charging pump.

The test conditions are determined by the stagnation pressure and temperature of the pressure vessel and the geometry of the test section. The pressure vessel, the pressure of which is maintained constant during the test, is a vertical vessel which has an inner diameter of 0.57 m, a length of 5.092 m, and a volume of 1.3 m^3. The connecting pipe which has an inner diameter of 87.3 mm and a length of 2.36 m is located below the pressure vessel and it is installed with a flow meter to measure the critical flow rate. There is gas injection/mixing piping into which the nitrogen gas is injected through a finely designed gas injection nozzle and in which it is mixed with the discharged coolant. The test section is located below this gas injection/mixing piping to measure the thermo-hydraulic parameters and it is connected to the discharge tank, which safely receives the discharged coolant.

2.2. Test section and instrument

The locations of the sensors installed in the test section of the critical flow test facility are listed in Table 1.

Table 1
The locations of the sensors installed in the critical flow test facility

Sensor ID	Location (m)
Pressure transmitters	
P0	−0.030
P1	0.003
P2	0.023
P3	0.093
P4	0.168
P5	0.250
P6	0.370
P7	0.500
P8	0.600
P9	0.680
P10	0.750
P11	0.810
P12	0.860
P13	0.910
P14	0.950
P15	0.990
P16	0.9995
PL	1.030
Thermocouples	
T0	−0.030
T1	0.100
T2	0.350
T3	0.650
T4	0.900
Gamma densitometer	
VF1	0.500

The test section, which is named T2, is a sharp-edged stainless steel pipe, which has an inner diameter of 10.9 mm, a thickness of 3.2 mm, and a length of 1000 mm. It is instrumented with five thermocouples and eighteen pressure taps to measure the distributions of the temperature and pressure. A twin test section to measure the void fraction has been designed and a single-beam gamma densitometer (Park et al., 2002) has been applied. The test section T2GDM is a stainless steel pipe, which has the same length and inner diameter as T2.

The instrumentation specifications of the critical flow test facility are shown in Table 2.

Table 2
The instrumentation specifications of the critical flow test facility

Location	Tag ID	Model and type	Calibration range	Error (%)	Remarks
Pressure vessel	PT102	Rosemount 3051PG5	0–120 bar	0.05	
	TE113	Watlow, K-type	0–400 °C	0.4	
Connecting line	FT301	Fisher–Rosemount, ProBar, PBR + 26S	0–42 kg/s	0.5	Calibrated at 120 bar, 320 °C
Gas injection line	FT202	Hoffer, Turbine flowmeter, HO Precision series	0.012–0.67 kg/s	2.0	Calibrated at 175 bar, 87.5 °C
	TG1	Watlow, K-type	0–400 °C	0.4	
Test section	P0	Rosemount 3051CG5	0–138 bar	0.05	Installed at T2
	P1–P16	Rosemount 3051CD4	0–20.7 bar	0.05	Installed at T2
	PL	Rosemount 3051CG4	0–20.7 bar	0.05	Installed at T2
	T0–T4	Watlow, K-type	0–400 °C	0.4	Installed at T2
	VF1	Single-beam gamma densitometer	0–1.0	10.0	Installed at T2 GDM

The stagnation temperature and pressure of the coolant are measured in the pressure vessel, and the coolant is discharged through the discharge pipe. Its flow rate is measured upstream of the test section. Also the temperature and the flow rate of the injected nitrogen gas through the injection nozzle are measured. By using test section T2 the pressure and temperature distributions are measured throughout the test section and by using test section T2GDM the local void fraction is measured with a single-beam gamma densitometer.

3. Experimental procedure and test matrix

3.1. Experimental procedure

The coolant is discharged from a pressure vessel, and nitrogen gas is injected into the test loop and mixed with the coolant, and the mixture flows into the discharge tank through the test section with a critical velocity. The detailed experimental procedure is as follows:

(1) The high-pressure nitrogen gas is stored in the nitrogen gas supply tank by using the nitrogen gas charging system.
(2) The pressure vessel is filled with water to the pre-determined level. The water is heated and circulated by using the installed heater and pump of the main circulation system until the pressure vessel has the pre-determined stagnation temperature.
(3) The nitrogen gas is injected into the pressure vessel to provide a stagnation pressure. The pressure is maintained constant by using the pressure control valve (PCV) which is connected to the nitrogen gas supply tank.
(4) When the experimental conditions are reached, the water is discharged from the pressure vessel at an early stage by opening a quick-opening valve (QOV). The QOV has a minimum opening time of 1.0 s.
(5) To simulate the flow of a non-condensable gas, nitrogen gas is injected upstream of the test section in the following stage. The flow of the nitrogen gas is controlled by a flow control valve (FCV) and the nitrogen gas flows into the nitrogen gas/mixing piping to be mixed with the discharged coolant.
(6) After the pressure vessel has reached the pre-determined pressure and temperature, the data acquisition system (DAS) starts. As the coolant level descends to below the pre-determined level in the pressure vessel, the experiment ends and the DAS stops. The steady-state data of the critical flow rate, the stagnation pressure, the stagnation temperature, and the void fraction are acquired.

3.2. Experimental test matrix

A total of 98 runs of the tests are performed by using the test sections of T2GDM and T2. During the tests the critical flow rate, and the pressure and temperature distributions or the void fraction are measured. The stagnation temperatures are at a normal condition, which means an atmospheric temperature condition, and 0, 20, and 50 °C subcooled conditions, and the stagnation pressures are 4.0, 7.0, and 10.0 MPa, respectively. Table 3 shows the experimental test matrix of the KAERI critical flow tests.

In the case when the stagnation temperature is in a normal condition, the numbers of acquired experimental data are 14 and 27 for the tests without a non-condensable gas and with a non-condensable gas injected, respectively. In the case when the stagnation temperature is in a saturated or a lower subcooled condition, the numbers of acquired experimental data are 21 and 36 for the tests without a non-condensable gas and with a non-condensable gas injected, respectively.

4. Results and discussion

A total of 23 and 75 experimental data results were acquired by using the test sections of T2 and T2GDM, respectively. It was ascertained that the same critical flow rates were measured by using T2 and T2GDM for the same test conditions. Tests were performed at the stagnation pressures of 4.0, 7.0, and 10.0 MPa, the

Table 3
The experimental test matrix for the KAERI critical flow tests

Experimental condition		Number of test case	
Stagnation pressure (MPa)	Stagnation temperature (°C)	Without NCG injection	With NCG injection
4.0	Saturated	2	1
	20 °C subcooled	1	1
	50 °C subcooled	3	6
	Normal temperature	5	12
7.0	Saturated	2	2
	20 °C subcooled	1	4
	50 °C subcooled	1	5
	Normal temperature	7	12
10.0	Saturated	2	2
	20 °C subcooled	6	9
	50 °C subcooled	3	6
	Normal temperature	2	3

stagnation temperatures of a normal, and a 0, 20, and 50 °C subcooled condition, and the nitrogen gas flow rates of 0.0–0.22 kg/s. The maximum experimental uncertainty of the measured critical flowrate was 13.0%.

4.1. Typical experimental data

The steady-state experimental data were acquired according to the experimental procedure. As the stagnation pressure of the pressure vessel and the flow rates of the injected nitrogen gas and the discharged coolant were maintained as constant, the steady-state condition was reached. Fig. 2 shows the typical experimental

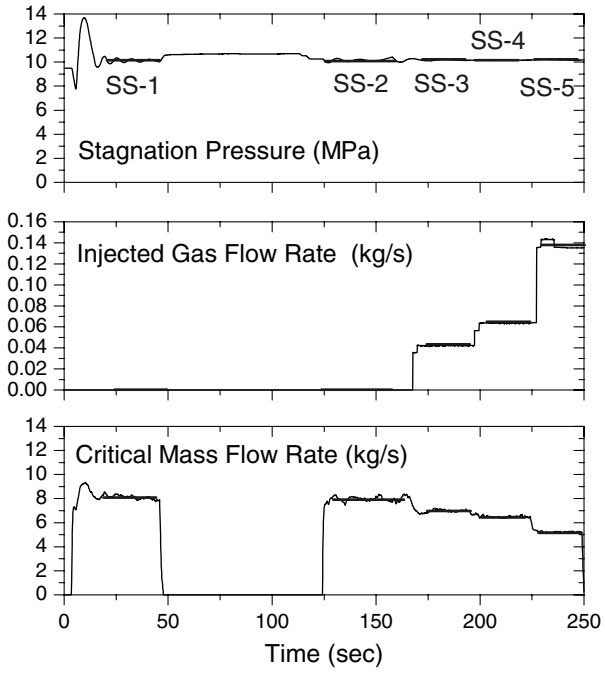

Fig. 2. Typical experimental results for the behaviors of the stagnation pressure of the pressure vessel and the flow rates of the injected nitrogen gas and the discharged coolant.

results for the behavior of the stagnation pressure of the pressure vessel and the flow rates of the injected nitrogen gas and the discharged coolant.

The test was performed at the stagnation pressure of 10.0 MPa and at a normal temperature. Two steady-state data results of SS-1 and SS-2 were acquired for the tests without a non-condensable gas, and three data results of SS-3, SS-4, and SS-5 were acquired for the tests with a non-condensable gas. The measuring intervals were 29.0, 40.4, 24.5, 25.0 and 19.0 s for the test cases of SS-1, SS-2, SS-3, SS-4, and SS-5, respectively.

Figs. 3 and 4 show the typical distributions of the pressure and temperature in the test section T2, respectively. The stagnation pressure and temperature were 10.0 MPa and 291 °C, respectively.

As shown in Fig. 3, most of the pressure drop occurred at the exit of the test section irrespective of the different injected nitrogen gas flow rates. As the injected nitrogen gas flow rate increased, the pressure drop increased throughout the whole test section. As shown in Fig. 4, the temperature decreased at the entrance of the test section, but it was recovered throughout the whole test section. The typical profiles of the pressure and temperature could be used to assess the simulation capabilities of the mechanistic models for the system analysis code.

A few experiments were performed by using T2GDM to acquire the experimental data of the critical flow rate and the void fraction. The volumetric void fraction upstream of the test section was calculated by using the flowrates of the discharged water and the injected nitrogen gas measured by separate flow meters, and the void fraction was estimated from the empirical correlation of Yamazaki and Yamaguchi (1979). The typical void fractions measured at the center of the test section by using a single-beam gamma densitometer were compared with those calculated from the volumetric void fractions upstream of the test section at a stagnation pressure of 7.0 MPa and an atmospheric temperature. The void fractions upstream of the test section were 0.1369 and 0.2171, and the corresponding void fractions measured by using a single-beam gamma densitometer were 0.2804 and 0.4835, respectively. The measured void fractions at the center of the test section always gave larger values than the initial void fractions, which can be explained in two ways. One is the Mishima and Ishii (1984)'s theory which shows that the probabilities of a coalescence are much higher for a small diameter tube of a test section than those with a larger diameter tube of a connecting pipe, which was also observed by Jiang and Rezkallah (1993). The other is due to the fact that the fluid in the test section is in a critical flow condition. In two-phase critical flow conditions, an additional void is generated near the outlet of the test section and it could affect an increase of the void fraction in the middle of a test section.

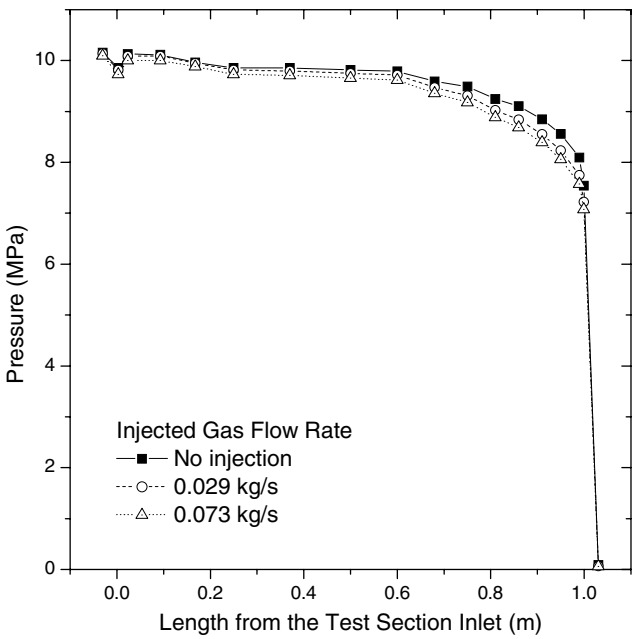

Fig. 3. Typical pressure distribution in test section T2.

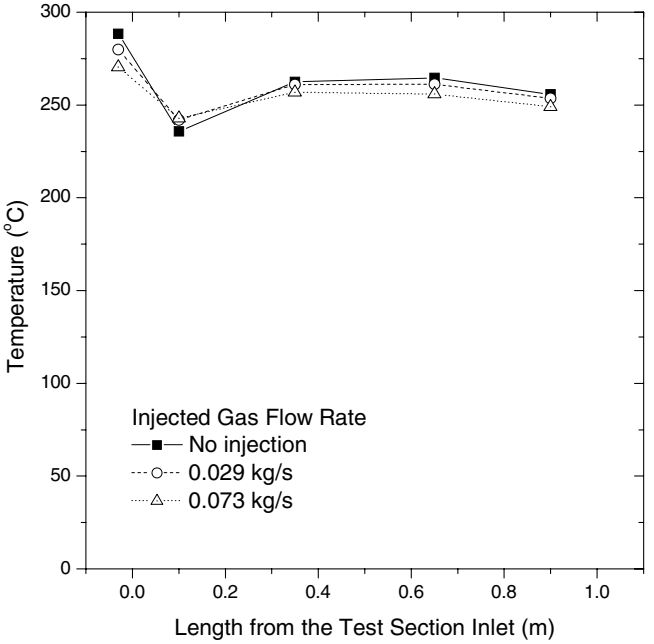

Fig. 4. Typical temperature distribution in test section T2.

4.2. Test results for the tests without a non-condensable gas

In the early stages, only the coolant water was discharged without an injection of the nitrogen gas, and in the latter stages the nitrogen gas was injected and mixed with the coolant with a pre-determined flow rate. After the discharged coolant was mixed with the injected nitrogen gas in the mixer, 0.8 m upstream of the test section inlet, it flowed into the test section. A mixture of the coolant and nitrogen gas was discharged into the suppression tank through the test section which had a total length of 1.0 m.

The critical mass flux versus the stagnation temperature for the three different stagnation pressures obtained by the present experiment without a non-condensable gas is plotted in Fig. 5.

The critical mass flux increased as the stagnation pressure increased and the stagnation temperature decreased as expected. The rate of the decrease of the mass flux became larger as the stagnation temperature became higher or when it had reached its saturation point.

Park (1997) developed two empirical correlations for the two-phase critical flow rates based on a total of 457 two-phase critical flow tests and the predictions from the developed correlations were compared with those of the commonly-used models to show their applicability to a one-component two-phase critical flow. Park (1997)'s correlation provides a simple and direct calculation of a critical mass flux, once the initial stagnation conditions and geometry of the flow channel are given. In Park (1997)'s empirical correlations the critical flow rate of a subcooled water is calculated in terms of a discharge coefficient of cold (20 °C) water $(C_d)_{ref}$ and a dimensionless subcooling ΔT^*_{sub}. The discharge coefficient and the dimensionless subcooling are defined as follows:

$$(C_d)_{ref} = \left(f\frac{L}{D} + K + 1\right)^{-0.5}_{ref} \tag{1}$$

$$\Delta T^*_{sub} = \frac{T_{sat} - T_0}{T_{sat} - T_{ref}} \tag{2}$$

where the subscripts ref, sub, sat, and 0 refer to the values of the water flow at 20 °C for the given pressure, and the subcooled, saturated, and stagnation conditions, respectively. f is the friction factor, L the total length, D the diameter, K the form loss coefficient, and T the temperature. In the case where the values of K and f are not

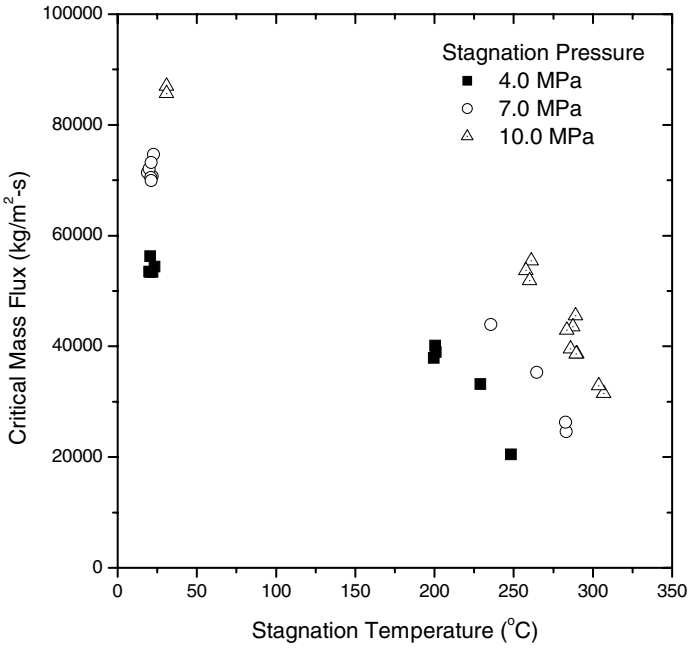

Fig. 5. The critical mass flux versus the stagnation temperature for the three different stagnation pressures obtained by present experiment without a non-condensable gas.

known to be accurate, $(C_d)_{ref}$ is calculated from the measured critical flow rate at the reference temperature condition.

For $L/D \geqslant 10$ with $L \geqslant 40$ mm, the critical mass flux can be calculated as a function of G_{ref} and ΔT^*_{sub} as in the following (Park, 1997):

$$G_c = G_{ref} \cdot \left[1 - \frac{15.2}{1 + \exp\{(\Delta T^*_{sub} + 0.578)/0.188\}}\right] \tag{3}$$

and

$$G_{ref} = (C_d)_{ref}\{2\rho(P_0 - P_b)\}^{0.5}_{ref} \tag{4}$$

where ρ is the density of the water, P_0 is the stagnation pressure, P_b is the backpressure of the suppression tank, G_{ref} is the reference mass flux, and G^* is the dimensionless mass flux defined as G_c/G_{ref}.

The dimensionless mass fluxes (G^*) versus the dimensionless subcooling (ΔT^*_{sub}) for all the experimental data without a non-condensable gas obtained from the present test section are plotted in Fig. 6 and they are compared with the values calculated by the empirical correlation developed by Park (1997).

For the stagnation pressure of 4.0 MPa, the agreement between the experimental data and the values predicted by the empirical correlation is very good. As the stagnation pressure increased the measured critical mass fluxes became smaller than those predicted by the empirical correlation of Park (1997), which was developed based on data with operating pressures below 2.0 MPa. There is a need to develop a more generalized correlation to include the critical flow data at a high pressure condition.

The mean relative difference ($\bar{x}$) between the data and the calculated values and the standard deviation (σ) were calculated for three different stagnation pressures. Here $\bar{x}$ and σ were defined by the following equations:

$$\bar{x} = \frac{1}{n}\sum_{i=1}^{n} x_i \tag{5}$$

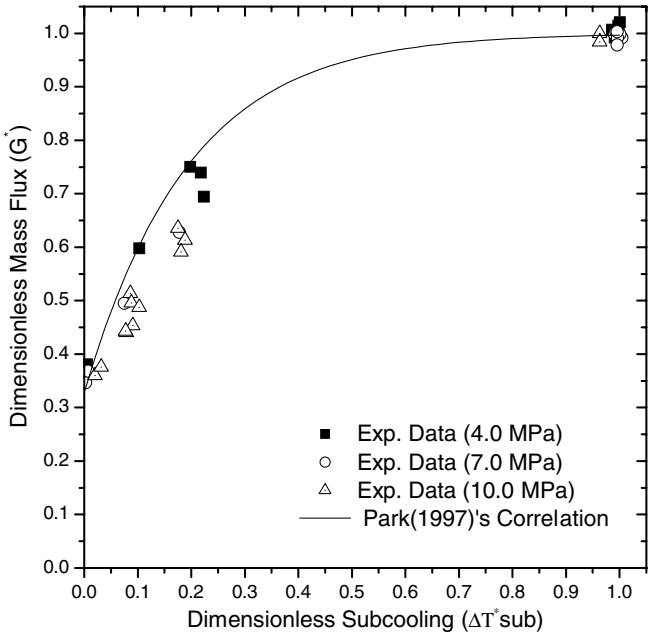

Fig. 6. The dimensionless mass fluxes versus the dimensionless subcooling obtained by the present experiment and those calculated by the empirical correlation of Park (1997).

where

$$x_i = \left(\frac{G_{\text{exp}} - G_{\text{cor}}}{G_{\text{exp}}}\right)_i \tag{6}$$

and

$$\sigma = \left(\sum_{i=1}^{n} \frac{x_i^2}{n-1}\right)^{0.5} \tag{7}$$

where n is the number of experimental data. The relative differences are −0.60, −1.85, −16.34% and the standard deviations are 5.88, 6.01, 9.15% for the stagnation pressures of 4.0, 7.0 and 10.0 MPa, respectively.

4.3. Test results for the tests with a non-condensable gas

Figs. 7–9 show the variations of the critical mass fluxes with a change of the non-condensable gas fraction when the stagnation temperature is at a normal temperature condition, at a 50 °C subcooled condition, and at a saturated condition, respectively.

The critical flow rate decreased rapidly with an increase of the non-dimensional volumetric flow rate of the non-condensable gas. The results show that the non-condensable gas fraction was an important parameter for predicting the critical flow rate.

Celata et al. (1988) performed experiments to study the influence of a non-condensable gas on a steam-water two-phase critical flow and based on their experimental data they proposed an empirical correlation for a dimensionless critical mass flux $R(=G_c/G_{c0})$ which is a function of a dimensionless volumetric flow rate of a non-condensable gas Q_a/Q_{c0} and an inlet subcooling ΔT_{sub} as follows:

$$R = \exp(0.00361 \cdot \Delta T_{\text{sub}} - 1.55 \cdot \sqrt{Q_a/Q_{c0}}) \tag{8}$$

where ΔT_{sub} is the water subccoling, G_c is the experimental critical mass flux, G_{c0} is the reference mass flux without a non-condensable gas, Q_a is the volumetric flow rate of the non-condensable gas, and Q_{c0} is the reference volumetric flow rate without a non-condensable gas.

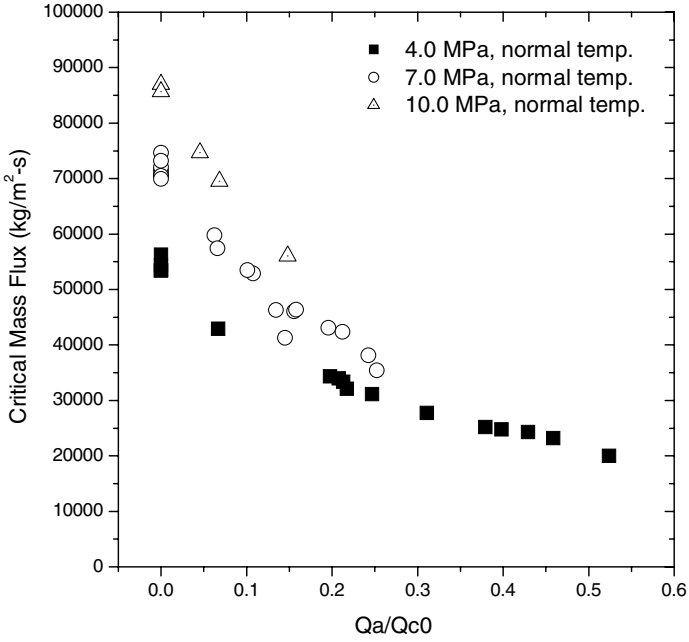

Fig. 7. Critical mass flux variation with a change of the non-condensable gas fraction in a normal temperature condition.

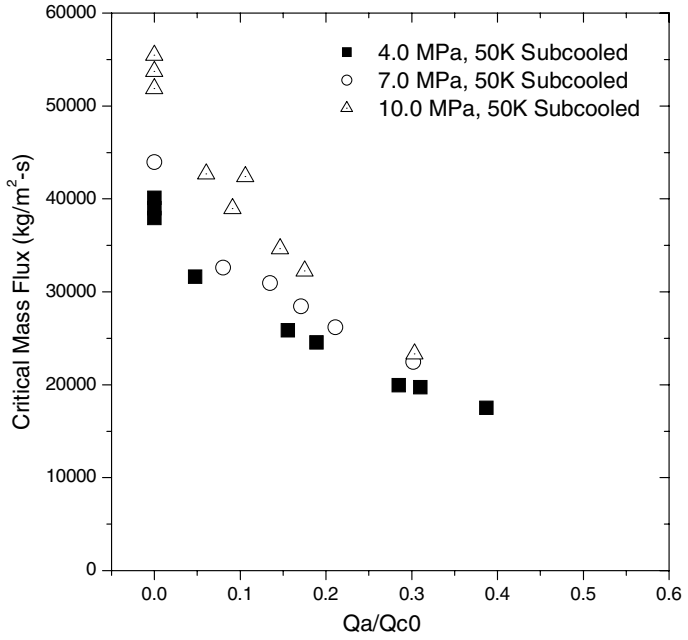

Fig. 8. Critical mass flux variation with a change of the non-condensable gas fraction in a 50 °C subcooled condition.

As shown in Figs. 7–9, the critical mass flux decreased rapidly as the non-condensable gas fraction increased. Also the critical mass flux increased as the stagnation pressure increased.

Fig. 10 shows the variation of the critical mass flux with a change of the non-condensable gas fraction at the stagnation pressure of 7.0 MPa. In the normal temperature condition the critical mass flux decreased rapidly with an increase of the non-condensable gas fraction. The decreasing rate was the smallest when the stagnation temperature was at a saturated condition.

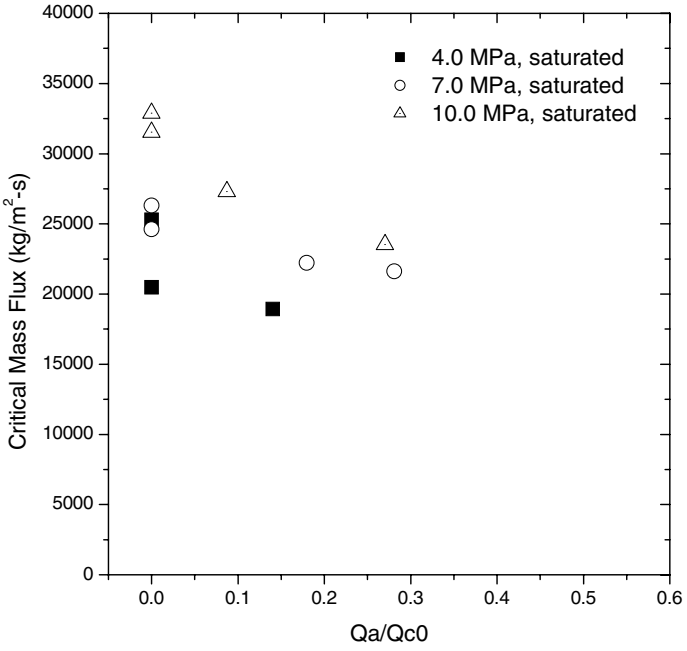

Fig. 9. Critical mass flux variation with a change of the non-condensable gas fraction in a saturated condition.

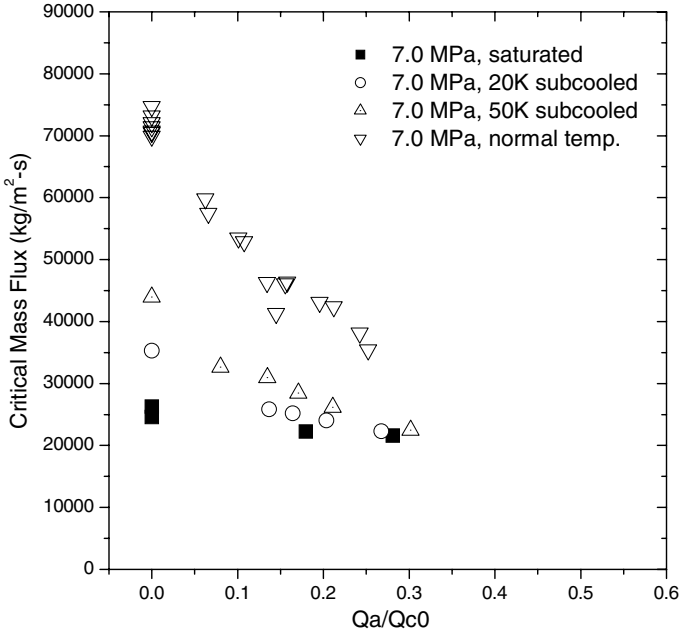

Fig. 10. Critical mass flux variation with a change of the non-condensable gas fraction at the stagnation pressure of 7.0 MPa.

An empirical correlation was developed based on the experimental data with a non-condensable gas except for the data at the saturated condition. In the operating ranges in this study, the dimensionless critical mass flux R was expressed with a function of the dimensionless volumetric flow rate of the non-condensable gas Q_a/Q_{c0} as follows:

$$R = 0.378 + 0.600 \cdot e^{-(Q_a/Q_{c0})/0.195} \tag{9}$$

Eq. (9) is applicable for the stagnation pressures of 3.7–10.5 MPa, the stagnation temperature range from 19.8 °C subcooled to a normal condition, and the non-condensable gas flow rates of 0.008–0.218 kg/s.

Fig. 11 shows the dimensionless critical mass flux versus the dimensionless volumetric flow rate of the non-condensable gas obtained by the present experiment and those calculated by the present and Celata et al.

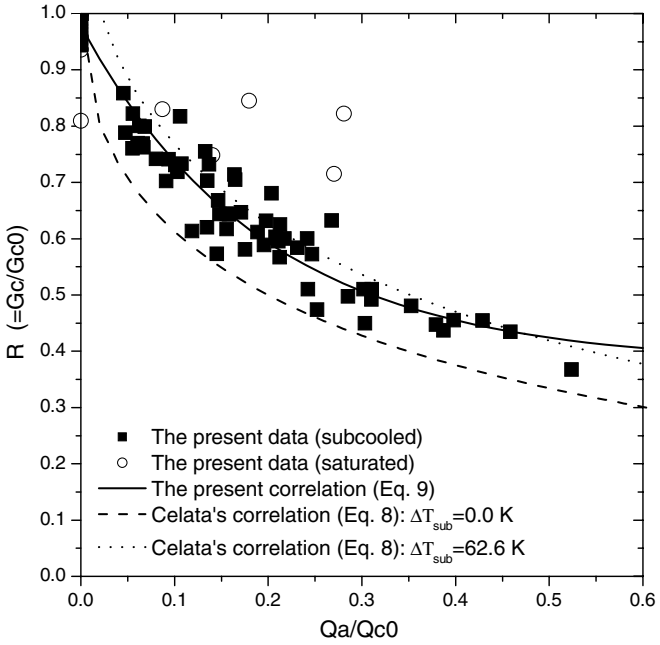

Fig. 11. The dimensionless critical mass flux versus the dimensionless volumetric flow rate of the non-condensable gas obtained by the present experiment and those calculated by the present and Celata et al. (1988)'s correlations.

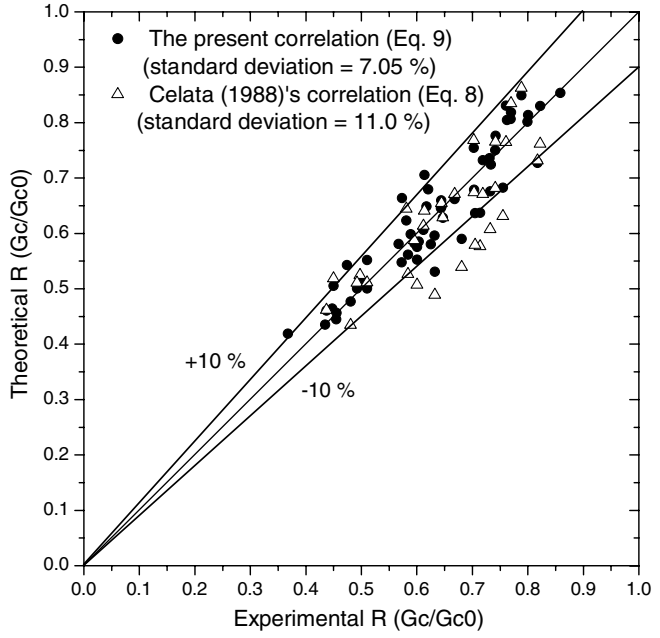

Fig. 12. Prediction results of the critical mass flux for the data with low subccoling using the present and Celata et al. (1988)'s empirical correlation.

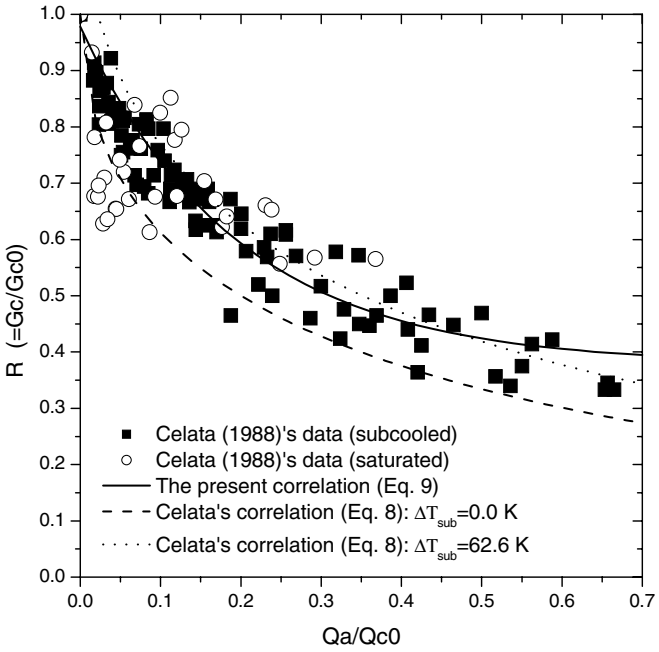

Fig. 13. The dimensionless critical mass flux versus the dimensionless volumetric flow rate of the non-condensable gas obtained by Celata et al. (1998) and those calculated by the present and Celata et al. (1988)'s correlations.

(1988)'s correlations. The predictions of the present correlation are similar to the experimental results except for the saturated condition. In the present correlation the non-condensable critical mass flux can be expressed as a function of the fraction of the volumetric flow rate of the non-condensable gas. The critical mass flux decreased rapidly with an injection of the non-condensable gas. The present experimental results show that the effect of an inlet subcooling was negligible for the investigated operating ranges. In the case of the saturated condition, the non-dimensional critical mass flux changes over a broad band, and the degradation effect of the non-condensable gas was smaller when compared with the case of the subcooled condition. In Celata et al. (1988)'s correlation, the critical mass fluxes are calculated based on two boundary values of a coolant subcooling of 0 and 62.6 K.

Fig. 12 shows the prediction results of the critical mass fluxes for the data with a low subcooling by using the present and Celata et al. (1988)'s empirical correlation. The standard deviation of the predictions of the present empirical correlation from the experimental values was 7.05%. Celata et al. (1988)'s correlation predicted the experimental values as a little lower with a standard deviation of 11.0% for the data with a low subcooling, but it predicted the experimental values as much higher for the data with a normal temperature.

Fig. 13 shows the dimensionless critical mass flux versus the dimensionless volumetric flow rate of the non-condensable gas obtained by Celata et al. (1988) and those calculated by the present and Celata et al. (1988)'s correlations. The relative differences of the present correlation were −2.74 and −7.34% and the standard deviations were 9.06 and 19.65% for the experimental data in the subcooled and saturated conditions, respectively. The results show that the relative difference and the standard deviation were high for the data at the saturated condition.

5. Conclusions

A set of experimental tests was performed to obtain the non-condensable gas two-phase critical flow data from a small diameter pipe with an inner diameter of 10.9 mm and with a sharp-edged inlet geometry at high pressure conditions. The test conditions were the stagnation pressures of 4.0, 7.0, 10.0 MPa, water subcoolings of 0.0, 20.0, 50 °C, and nitrogen gas flow rates of 0.0–0.22 kg/s. The following conclusions have been reached from the experimental results:

1. As the stagnation pressure and the inlet subcooling increased, the critical mass flux increased.
2. The critical mass flux decreased rapidly with an increase of the non-dimensional volumetric flow rate of the non-condensable gas. It revealed that the non-condensable gas fraction is an important parameter for predicting a critical mass flux.
3. Based on the experimental data without a non-condensable gas, Park (1997)'s empirical correlation for the critical mass flux was evaluated. The agreement between the experimental data and the correlated value was reasonably good for a relatively lower stagnation pressure of 4.0 MPa. Therefore, a broad range of experimental data is necessary for the high pressure conditions.
4. Based on the experimental data with a non-condensable gas at the subcooled condition, an empirical correlation of the non-dimensional critical mass flux was developed, which can be expressed by a function of the non-dimensional volume flow rate of the non-condensable gas. The developed empirical correlation predicts the Celata et al. (1988)'s dimensionless critical mass flux for the subcooled condition better than that for the saturated condition.

From this study it is recommended that a broad range of data for a critical mass flux with a non-condensable gas is necessary to develop reliable correlations, especially for the saturated and the high pressure conditions.

References

Celata, G.P., Cumo, M., D'Annibale, F., Farello, G.E., 1988. The influence of non-condensible gas on two-phase critical flow. Int. J. Multiphase Flow 14, 175–187.

Chang, M.H., Yeo, J.W., Zee, S.Q., et al., 2002a. Basic Design Report of SMART, KAERI Report. KAERI/TR-2142/2002, Korea.

Chang, S.K., Park, H.S., Chung, C.H., 2002b. Two-phase critical flow with non-condensable gas on sharp-edged short pipe geometry. In: Proceedings of the Korea Nuclear Spring Meeting, Gwangju, Korea, May 23–24.

Choi, K.Y., Park, H.S., Cho, S., Yi, S.J., Park, C.K., Song, C.H., Chung, M.K., 2006. Parametric studies on thermal hydraulic characteristics for transient operations of an integral type reactor. Nucl. Eng. Technol. 38, 185–194.

Elias, E., Lellouche, G.S., 1994. Two-phase critical flow. Int. J. Multiphase Flow 20 (Suppl.), 91–168.

Fauske, H.K., 1985. Flashing flows or: some practical guidelines for emergency releases. Plant/Operations Progress 4, 132–134.

Henry, R.E., 1970. The two-phase critical discharge of initially saturates or subcooled liquid. Nucl. Sci. Eng. 41, 336–342.

Jiang, Y., Rezkallah, K.S., 1993. An experimental study of the suitability of using a gamma densitometer for void fraction measurements in gas-liquid flow in a small diameter tube. Mes. Sci. Technol. 4, 496–505.

Kim, S.H., Lim, H.S., Kim, H.C., 2002. Development and assessment of two-phase critical flow model with non-condensible gas. In: Proceedings of the Korea Nuclear Spring Meeting, Gwangju, Korea, May 23–24.

Mishima, K., Ishii, M., 1984. Flow regime transition criteria for upward two-phase flow in vertical tubes. Int. J. Heat Mass Transf. 27, 723–737.

Moody, F.J., 1965. Maximum flow rate of single component two-phase mixture. ASME J. Heat Transf. 86, 134–142.

Park, C.K., 1997. An experimental investigation of critical flow rates of subcooled water through short pipes with small diameters. Ph.D. Thesis, Korean Advanced Institute of Science and Technology, Korea.

Park, H.S., Chang, S.K., Chung, C.H., Lee, S.J., 2002. Void fraction measurements in a small diameter stainless steel pipe in critical flow conditions using a single-beam gamma densitometer. The 13th Pacific Basin Nuclear Conference (PBNC-2002), Shenzhen, China, October 21–25.

Pinhasi, G.A., Dayan, A., Ullmann, A., 2005. Modeling of flashing two-phase flow. Rev. Chem. Eng. 21, 133–264.

Trap, J.A., Ransom, V.H., 1982. A choked-flow calculation criterion for nonhomogeneous, nonequilibrium, two-phase flows. Int. J. Multiphase Flow 8, 669–681.

Wallis, G.B., 1980. Critical two-phase flow. Int. J. Multiphase Flow 6, 97–112.

Yamazaki, Y., Yamaguchi, K., 1979. Characteristics of cocurrent two-phase downflow in tubes – flow pattern, void fraction and pressure drop. J. Nucl. Sci. Technol. 16, 245–255.